



**HAL**  
open science

## Migration of finite sized particles in a laminar square channel flow from low to high Reynolds numbers

Micheline Abbas, Pascale Magaud, Y. Gao, Sandrine Geoffroy

► **To cite this version:**

Micheline Abbas, Pascale Magaud, Y. Gao, Sandrine Geoffroy. Migration of finite sized particles in a laminar square channel flow from low to high Reynolds numbers. *Physics of Fluids*, 2014, 26 (12), pp.123301. 10.1063/1.4902952 . hal-01850763

**HAL Id: hal-01850763**

**<https://hal.insa-toulouse.fr/hal-01850763>**

Submitted on 20 May 2019

**HAL** is a multi-disciplinary open access archive for the deposit and dissemination of scientific research documents, whether they are published or not. The documents may come from teaching and research institutions in France or abroad, or from public or private research centers.

L'archive ouverte pluridisciplinaire **HAL**, est destinée au dépôt et à la diffusion de documents scientifiques de niveau recherche, publiés ou non, émanant des établissements d'enseignement et de recherche français ou étrangers, des laboratoires publics ou privés.



## Open Archive Toulouse Archive Ouverte (OATAO)

OATAO is an open access repository that collects the work of some Toulouse researchers and makes it freely available over the web where possible.

This is an author's version published in: <http://oatao.univ-toulouse.fr/20230>

**Official URL:** <http://doi.org/10.1063/1.4902952>

### To cite this version:

Abbas, Micheline and Magaud, Pascale and Gao, Yanfeng and Geoffroy, Sandrine Migration of finite sized particles in a laminar square channel flow from low to high Reynolds numbers. (2014) *Physics of Fluids*, 26 (12). 1-12. ISSN 1070-6631

Any correspondence concerning this service should be sent to the repository administrator:

[tech-oatao@listes-diff.inp-toulouse.fr](mailto:tech-oatao@listes-diff.inp-toulouse.fr)

# Migration of finite sized particles in a laminar square channel flow from low to high Reynolds numbers

M. Abbas,<sup>1,2,a)</sup> P. Magaud,<sup>2,3</sup> Y. Gao,<sup>3</sup> and S. Geoffroy<sup>2,4</sup>

<sup>1</sup>Laboratoire de Génie Chimique, Université de Toulouse INPT-UPS, 31030, Toulouse, France

<sup>2</sup>CNRS, Fédération de recherche FERMaT, CNRS, 31400, Toulouse, France

<sup>3</sup>Institut Clément Ader, Université de Toulouse UPS-INSA-ISAE-Mines Albi, 31400, Toulouse, France

<sup>4</sup>Laboratoire Matériaux et Durabilité des Constructions, Université de Toulouse; UPS, INSA, 31077, Toulouse, France

The migration of neutrally buoyant finite sized particles in a Newtonian square channel flow is investigated in the limit of very low solid volumetric concentration, within a wide range of channel Reynolds numbers  $Re = [0.07-120]$ . *In situ* microscope measurements of particle distributions, taken far from the channel inlet (at a distance several thousand times the channel height), revealed that particles are preferentially located near the channel walls at  $Re > 10$  and near the channel center at  $Re < 1$ . Whereas the cross-streamline particle motion is governed by inertia-induced lift forces at high inertia, it seems to be controlled by shear-induced particle interactions at low (but finite) Reynolds numbers, despite the low solid volume fraction ( $<1\%$ ). The transition between both regimes is observed in the range  $Re = [1-10]$ . In order to exclude the effect of multi-body interactions, the trajectories of single freely moving particles are calculated thanks to numerical simulations based on the force coupling method. With the deployed numerical tool, the complete particle trajectories are accessible within a reasonable computational time only in the inertial regime ( $Re > 10$ ). In this regime, we show that (i) the particle undergoes cross-streamline migration followed by a cross-lateral migration (parallel to the wall) in agreement with previous observations, and (ii) the stable equilibrium positions are located at the midline of the channel faces while the diagonal equilibrium positions are unstable. At low flow inertia, the first instants of the numerical simulations (carried at  $Re = O(1)$ ) reveal that the cross-streamline migration of a single particle is oriented towards the channel wall, suggesting that the particle preferential positions around the channel center, observed in the experiments, are rather due to multi-body interactions. © 2014 AIP Publishing LLC. [<http://dx.doi.org/10.1063/1.4902952>]

## I. INTRODUCTION

In the field of suspension flows, the pioneering experiments of Segré and Silberberg<sup>1</sup> highlighted the fact that neutrally buoyant finite sized particles migrate across the tube flow streamlines towards an equilibrium ring located at  $r = 0.6R$  ( $R$  being the tube radius). After these observations, many theoretical studies tackled the problem of inertia-driven particle migration in order to determine the origin of this phenomenon.<sup>2-6</sup> All the evidence suggests that the particle cross-streamline migration is related to the interaction of the particle Stresslet (rigidity constraint of the finite sized particle) with the curved velocity profile of the pressure-driven flow, and that the speed of the migration process, as well as the particle equilibrium positions, depends exclusively on the Reynolds number and on the particle-to-channel (or tube) size ratio.

---

<sup>a)</sup> Author to whom correspondence should be addressed. Electronic mail: [micheline.abbas@ensiacet.fr](mailto:micheline.abbas@ensiacet.fr)

In the last decade, the particle migration due to flow inertia has been extensively used for successful particle separation and sorting in microfluidic devices.<sup>7-9</sup> Square channels are often considered due to the ease of their manufacturing process. However, it is complex to establish theoretical predictions of the particle-flow interaction in rectangular 3D flow geometries. At finite inertia, the experiments and numerical simulations agree on the fact that, in a square channel flow, particles first undergo a cross-streamline migration (similarly to the Segré-Silberberg phenomenon) until they reach an equilibrium ring parallel to the velocity iso-contours (see Figure 8(a)). This is followed by a cross-lateral migration along the equilibrium ring that is proper to rectangular channel flows with small aspect ratios (there is no such type of spanwise motion in axisymmetric pipe or plane Poiseuille flow). At present, one cannot find a universal agreement on the location of the stable particle positions at the equilibrium ring. The experiments performed in microsystems, in the range  $Re = [1-120]$ , show that equilibrium positions may be found in the corners<sup>8</sup> as well as in the midline of the channel walls<sup>7,9</sup> ( $Re = \langle U \rangle H / \nu$ , where  $\langle U \rangle$ ,  $H$ , and  $\nu$  are the average flow velocity, channel height, and fluid kinematic viscosity, respectively). In parallel, numerical simulations of freely moving particles revealed the existence of several equilibrium positions along the ring.<sup>10</sup> Later this information was refuted by the numerical simulations of Di Carlo *et al.*,<sup>11</sup> who considered a single fixed particle while the boundary conditions of the channel were modified in order to mimic the case of a freely moving particle. The authors showed that the amplitude of the lift force was canceled out only at the point attractors in the centers of the channel faces, suggesting that other equilibrium positions on the ring are unstable.

The fact that the literature lacks experimental observations at low inertia is likely due to the small inertia-driven cross-streamline migration velocities and consequently the very long channels necessary to observe particle trajectory deviation and potential preferential positions. From the theoretical calculation of the disturbance produced by a finite sized particle in a plane Poiseuille flow at finite but low inertia,<sup>2,3</sup> it is expected, though, that a single particle located close to the channel center would migrate towards the wall.

In order to assess the applicability of the inertial migration prediction in square channel geometry and in a dilute suspension flow (such as it is practiced in particle or cell sorting applications), we performed experiments and numerical simulations within a wide range of Reynolds numbers. Section II provides information on the experimental and numerical tools used for the present investigation. The experimental results are shown in Sec. III, where different migration regimes are discerned. Whereas the inertia-driven migration is dominant at relatively high inertia, the shear-induced particle interactions seem to control the particle cross-streamline motion at low Reynolds numbers, even at very low concentration. To exclude the effect of hydrodynamic interactions, the trajectories of freely moving single particles is obtained thanks to the numerical simulations, and some features of particle dynamics are described in Sec. IV. At the end, Sec. V contains concluding remarks.

## II. EXPERIMENTAL AND NUMERICAL SETUPS

### A. Experimental setup

The experimental device consisted of square borosilicate channels of  $H = 80 \mu\text{m}$  inner height and 10 cm long. Figure 1(a) shows the square cross-section visualized by scanning electron microscopy. The inlet of the square channel was linked, with a silicone tube (ID  $\sim 1$  mm), to a stainless steel syringe pump (PDH 4400, Harvard Apparatus). This syringe pump was filled with the liquid-solid suspension without any trapped air bubbles and was used to generate a flow in the channel at rates ranging from 0.5 to 800  $\mu\text{l}/\text{min}$  corresponding to  $Re = [0.07-120]$ . The downstream end of the test channel was open to the atmosphere.

The particles were polystyrene microspheres (Interfacial Dynamics Corporation<sup>®</sup>) of diameter  $d_p = 8.7 \mu\text{m}$  ( $d_p/H = 0.11$ ) and density  $\rho_p = 1050 \text{ kg m}^{-3}$ . They were introduced at a solid volume fraction of 0.2%. The fluid was a mixture of glycerol 23% and deionized water 77%. The dynamic viscosity of this mixture was  $1.5 \times 10^{-3} \text{ Pa}\cdot\text{s}$  at room temperature. A perfect matching of the fluid with the particle density was respected in order to achieve the neutrally buoyant condition.

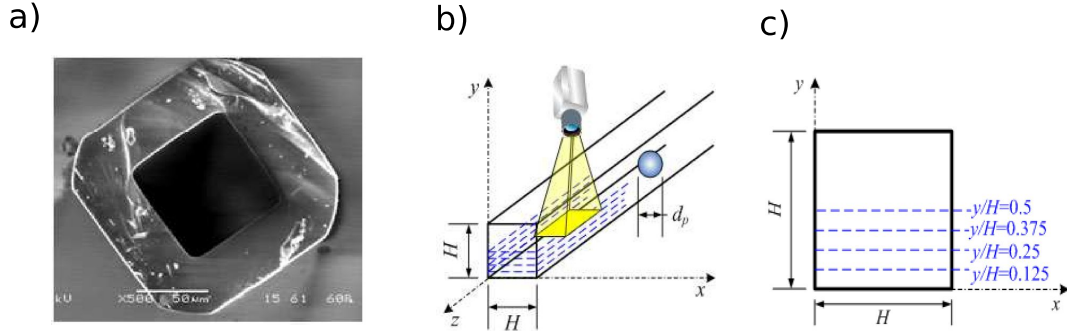


FIG. 1. (a) Image of the channel cross-section taken by scanning electron microscopy. (b) Scheme of the experimental setup. (c) Different positions of the focal plane.

A microscope equipped with an external light source (Leica EL6000) was used. The objective lens (X20 with numerical aperture 0.4) of the microscope was successively focused on different heights between the top and the bottom walls of the channel (as shown in Figure 1(b)). The depth of the field focus calibrated by static particles monitoring was of  $10 \mu\text{m}$ . At a given distance from the channel inlet, top view images were taken at seven different heights in the cross-section ( $y/H$  was varied from 0.125 to 0.875 with a step of 0.125), using a CCD camera (Sensicam with a resolution  $1376 \times 1040$  pixels). For each Reynolds number, 2000 images were saved to yield converged statistical results. The image acquisition was realized at 10 images per second, and the exposure time was varied from 1 to  $5 \mu\text{s}$ . We checked that the system reached a steady state before the onset of image acquisition.

The original gray-scaled images (Figure 2(a)) were then post-processed with Matlab. A background subtraction operation was performed allowing clearer particle identification (Figure 2(b)). Binary images (Figure 2(c)) were used to extract and filter contours against surface and shape (Figure 2(d)). In an image frame, one can observe both in-focus particles (particles with a bright point) and out-of-focus particles (particles with no bright point). Particles out-of-focus were eliminated in (Figure 2(e)). The positions of particle centers obtained from the 2000 recorded images were then collected on one reference image (Figure 2(f)), which led to a particle distribution function (Figure 3). The probability density function (PDF) at a given  $Re$  and  $z/H$  was obtained by normalizing the number of particles detected at a given height  $y/H$  by the total number of particles detected at all heights.

## B. Numerical method

The numerical method is based on the full coupling between the Navier-Stokes equations and the Lagrangian tracking of particles via the force coupling method.<sup>12</sup> The force coupling method is

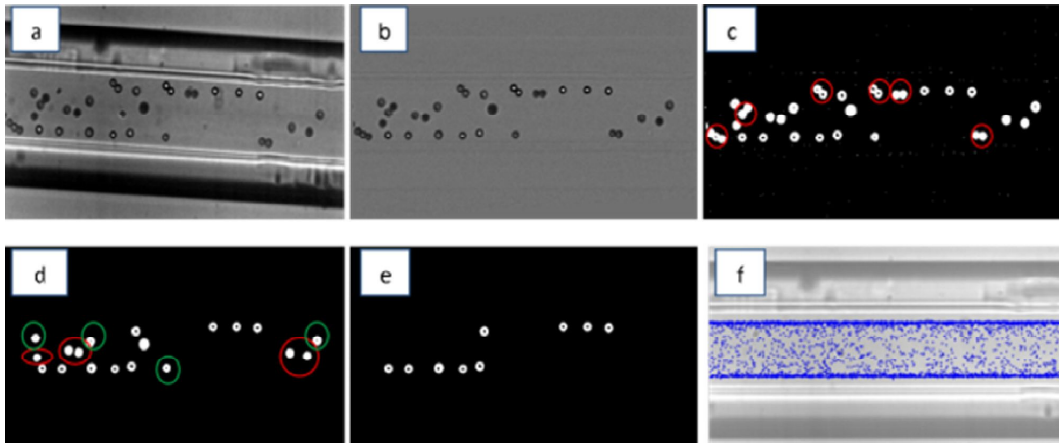


FIG. 2. Image processing steps.

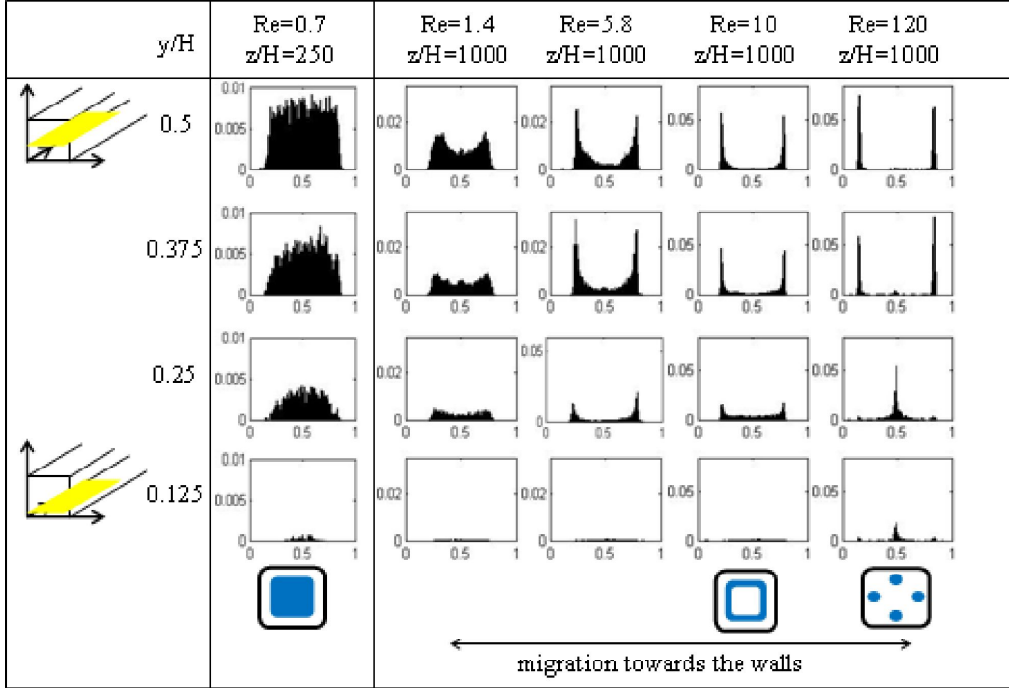


FIG. 3. PDF of particle positions along the channel width ( $x/H$ ) at different depths ( $y/H$ ) and distances ( $z/H$ ) from the channel inlet, and for different Reynolds numbers and  $\phi = 0.2\%$ . The results are perfectly symmetric with respect to the channel median plane, only the PDFs at  $y/H \leq 0.5$  are shown. A scheme of the particle distribution in the cross-section is also sketched at the bottom of the figure.

not a fully resolved direct numerical simulation in the sense that the no-slip boundary condition is not directly imposed at the surface of the particles. Instead, it is based on a low-order, finite force multipole representation of the particles in the flow. The main advantage of using the force coupling method is that it allows capturing the particle-flow interaction in a shear flow with a moderate computation cost. The equations that are solved as well as the numerical scheme are described in Loisel *et al.*<sup>13</sup> We mention in this section only relevant points related to the simulations carried for this work.

In the absence of external forces (no gravity effect on the neutrally buoyant particles), the coupling between the particles and the carrier fluid occurred exclusively because of the particle rigidity constraint. The symmetric Stresslet tensor, that ensures zero average strain in the particle volume, is composed of nine components which were computed iteratively. During the migration stages, the elements of the Stresslet tensor were finite due to the multiple shear directions and to finite (particle-induced) normal stresses at finite Reynolds numbers. These elements were successfully computed in less than three iterations per time step, using the conjugate gradient method.

The numerical scheme was validated in two cases which are described in details in Loisel *et al.*<sup>13</sup> First, a single particle was placed in a pure shear flow, and the shear and normal Stresslet values were in a very good agreement with the direct numerical simulation results of Mikulencak and Morris<sup>14</sup> provided that the Reynolds number was below 10. In the second case, a single particle was placed in a plane Poiseuille flow at finite flow inertia. Particle trajectories were obtained in a wide range of channel Reynolds numbers  $Re = [100-1500]$  corresponding to a particle Reynolds number in the range  $Re_p = [0.1-5]$ . The particle equilibrium positions were found to be in agreement with the theoretical development of Asmolov<sup>5</sup> based on the matched asymptotic expansions.

The simulations used for this work were performed with four grid points per particle radius in a square channel of dimensions  $(9 \times 9 \times 14.4)d_p^3$  (if not otherwise stated). Periodicity and no-slip conditions were imposed, respectively, in the streamwise direction and on the channel walls. The time step was  $0.04 t_s$  ( $t_s = d_p/2\langle U \rangle$ ). All simulations were performed within the range of validity of the numerical method (the particle Reynolds number based on the local shear is below 10).

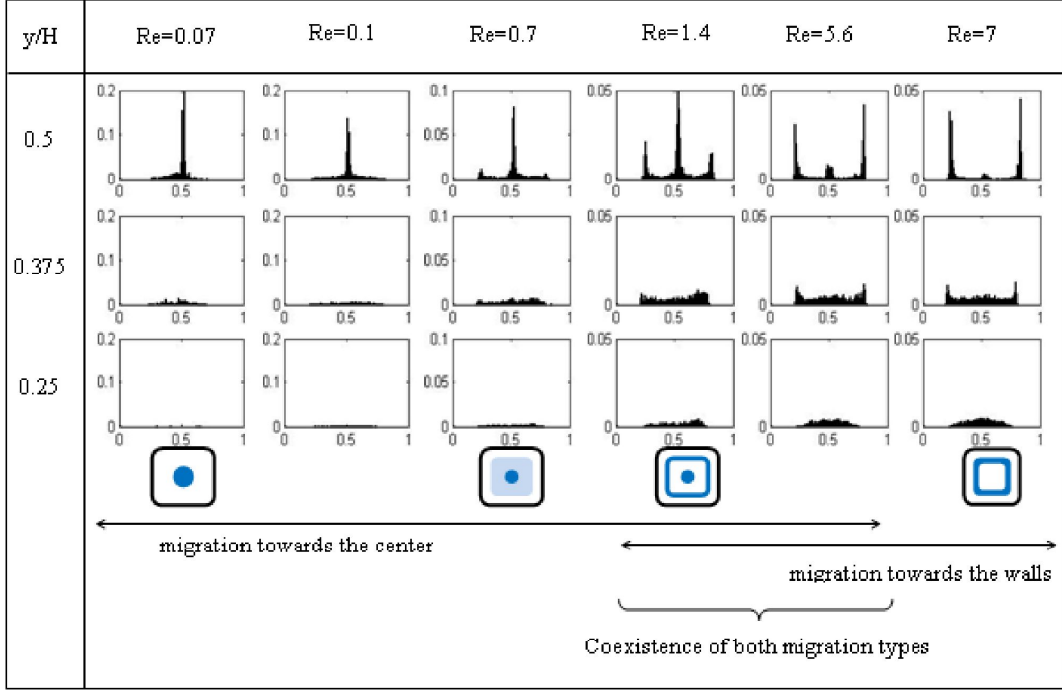


FIG. 4. *Idem* Figure 3 at  $z/H = 7215$  and lower Reynolds numbers.

### III. MIGRATION REGIMES FROM WEAK TO FINITE INERTIA

The PDFs presented here were computed at different  $Re$ , depths  $y/H$ , and streamwise distances from the channel inlet ( $z/H$ ). Figures 3 and 4 contain an overview of the different experimental results. In summary, close to the channel inlet, the particles were homogeneously distributed in the cross-section (see  $Re = 0.7$  and  $z/H = 250$ ). Far from the channel inlet, the particles were preferentially found at the center of the channel at  $Re \leq 1.4$ , whereas they were rather located close to the channel walls at  $Re \geq 10$ . Consequently, particle cross-streamline migration was controlled by distinct mechanisms when the Reynolds number was varied in the considered range.

#### A. Inertial particle migration

In the upper range of Reynolds number ( $Re > 1$ ), the particle migration is controlled by inertia. In this case, particles undergo cross-streamline migration due to the Segré-Silberberg phenomenon. The depletion of the channel center from particles is increased as the Reynolds number increases. At  $Re \geq 10$ , when the equilibrium between the inertia-induced lift force and the wall-induced hydrodynamic repulsion is reached, the particles are spread on a ring almost parallel to the channel walls (as shown by the PDFs at  $Re = 10$  and  $z/H = 1000$ ). For quantitative validation of the measurements, we calculated the distance between this ring and the channel walls using the location of the peaks in the histograms at the mid-section ( $y/H = 0.5$  and  $z/H = 1000$ ). The evolution of this distance as a function of  $Re$  is reported in Figure 8(b) and it will be commented in Sec. IV. The peak detected at the midline of the channel face ( $y/H = 0.25$  and  $z/H = 1000$ ) at  $Re = 120$  suggests that particles are also subject to cross-lateral migration on the equilibrium ring (in agreement with the observations of Choi *et al.*<sup>9</sup>). The cross-lateral migration will be discussed in details in the case of freely moving particles (in Sec. IV).

#### B. Particle migration at low inertia

In the lower range of Reynolds number ( $Re < 1$ ), the particles clearly migrate towards the channel center, and the process is very slow. At  $z/H = 1000$ , the regions close to the walls are particle free, but the PDFs are still uniform in the channel core (see Figure 3). Only very far from

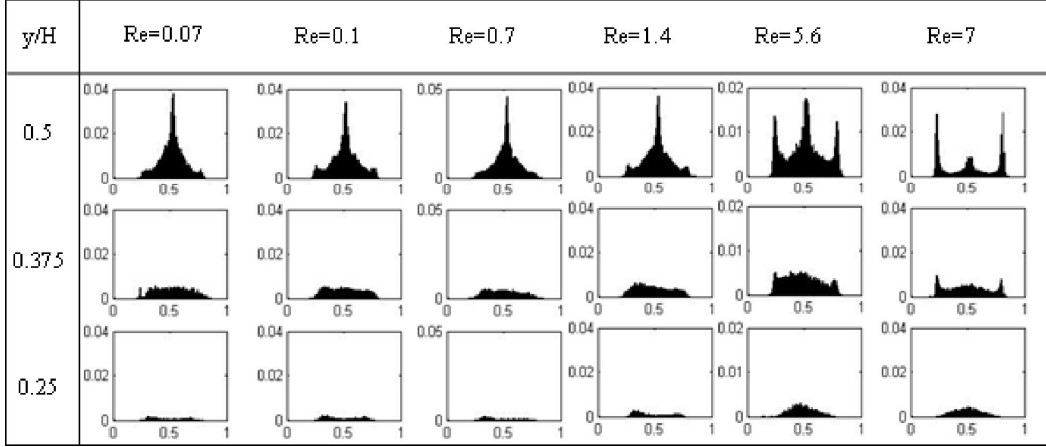


FIG. 5. *Idem* Figure 3 at  $z/H = 7215$  and  $\phi = 0.8\%$ .

the channel inlet (at  $z/H \geq 3000$ ), preferential positions start to be perceptible near the channel center (see Figure 4).

In the limit of negligible inertia at the particle scale (Stokes flow), it can be shown with reversibility arguments that a spherical single particle cannot exhibit any cross-streamline migration in the channel flow.<sup>15</sup> At weak but not negligible flow inertia, the finite sized particle is subject (in a plane Poiseuille flow) to a lift force that scales as the particle Reynolds number and that is oriented towards the channel wall when the particle is close to the channel center.<sup>2,3</sup> In order to have a prediction of the particle cross-streamline motion in the square channel flow at low inertia, we carried numerical simulations of a single particle at  $Re = O(1)$ . The first instants of particle trajectories showed that a single particle (placed close to the channel centerline) migrates towards the channel wall, in agreement with the theoretical results in plane Poiseuille flow. Unfortunately, it was not possible to obtain the complete particle trajectories, at low inertia, within a reasonable physical time, because the time step dropped drastically at  $Re < 5$ , and the migration velocities were very small.

These experimental and numerical observations suggest that the particle motion towards the channel center can be only due to the interactions between the particles. The shear-induced migration (which constitutive models were written in details for Couette and Poiseuille flows for instance in the work of Phillips *et al.*<sup>16</sup>) has been observed in several experiments in the case of confined suspension flows with both Brownian and non-Brownian particles at moderate to large concentration (see, for example, the works of Han *et al.*<sup>17</sup> at finite inertia and Semwogerere *et al.*<sup>18</sup> in Stokes flow). When the particle size is finite with respect to the channel height, the shear-induced migration results from the shear gradient at the particle scale: particles at different streamlines exhibit non-uniform collision frequency, which generate a net flux towards the lower shear rate regions. In this case, the cross-streamline migration flux is proportional to  $(d_p\phi)^2$ .

In order to check if the trend observed in the experiments is consistent with a shear-induced mechanism, we tested several particle radii and solid volume fractions, and compared the particle distributions with the reference case ( $\phi = 0.2\%$  and  $d_p/H = 0.11$ ), at one distance from the channel inlet ( $z/H = 7215$ ). When the suspension concentration increases, the percentage of particles found around the channel center is increased {see, for example, Figure 5 for  $\phi = 0.8\%$  and  $d_p/H = 0.11$ }.<sup>19</sup> On the contrary, when smaller particle size is used, the migration towards the center is weakened {see Figure 6 for  $\phi = 0.2\%$  and  $d_p/H = 0.0625$ }. Figures 5 and 6, in addition to complementary tests (not shown here), confirm qualitatively the increase, with the concentration and particle size, of the particle flux towards the center.

### C. Transition between both regimes

At intermediate  $Re$ ,  $1 \leq Re \leq 10$  and very far from the channel inlet, peaks near the walls and in the channel center seem to coexist. In this case, the inertial particle migration is strong enough



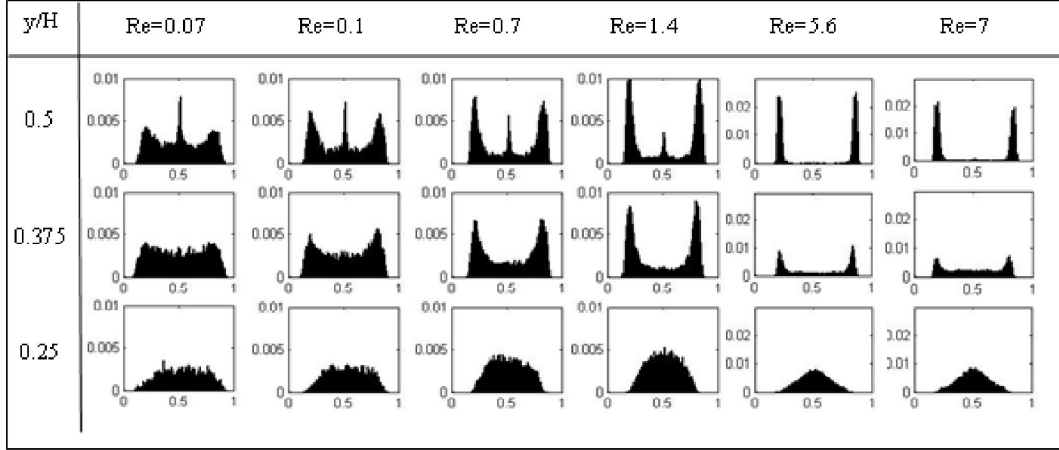


FIG. 6. *Idem* Figure 3 at  $z/H = 7215$ ,  $a/H = 0.0625$ , and  $\phi = 0.2\%$ .

to compete with the opposite collision-driven migration, both mechanisms being very slow. The particle positions, observed in this range, result from the competition between both phenomena, and therefore depend upon the distance of the measurement section with respect to the channel inlet. Taking the example of  $Re = 5.6$  (Figure 7), the particle motion seems to be controlled by inertia at  $\phi = 0.2\%$  and  $\phi = 0.8\%$  for  $z/H \leq 5000$ , whereas the shear-induced migration prevails further downstream at  $\phi = 0.8\%$ . In addition to the distance with respect to the channel inlet, Figures 4–6 clearly indicate that the transition between both migration regimes shifts towards higher  $Re$  when the concentration or particle size increase.

#### IV. DESCRIPTION OF SINGLE PARTICLE TRAJECTORIES IN THE INERTIAL REGIME

Numerical simulations of single particle motion allowed excluding the effect of particle interactions and focusing on the inertia-driven migration of the finite-sized particles in the square channel flow. Single particles were initially seeded at different locations in the channel cross-section. Figure 8(a) shows the projection of particle trajectories onto the velocity gradient plane. The black and green trajectories were obtained at  $Re = 120$ . One can clearly identify the two stages of inertial particle migration: a cross-streamline migration orthogonal to the velocity streamlines, followed by a particle motion along the equilibrium ring oriented towards the midline plane. The velocity in the second stage is one order of magnitude smaller than the inertial velocity. Particles initially placed in

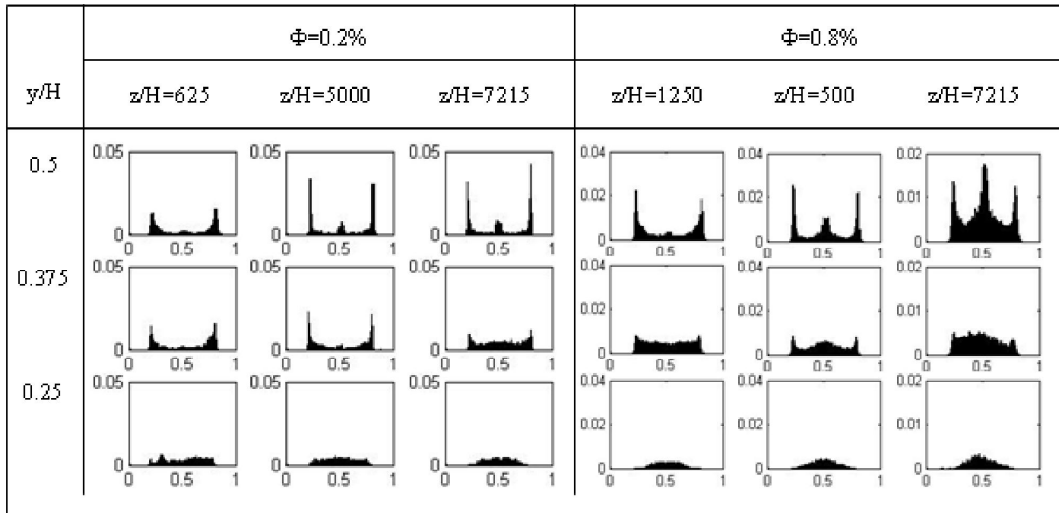


FIG. 7. Particle distributions at  $Re = 5.6$  showing the transient evolution of particle migration in the streamwise direction and the competition between the inertial and shear-induced migration for different concentrations.

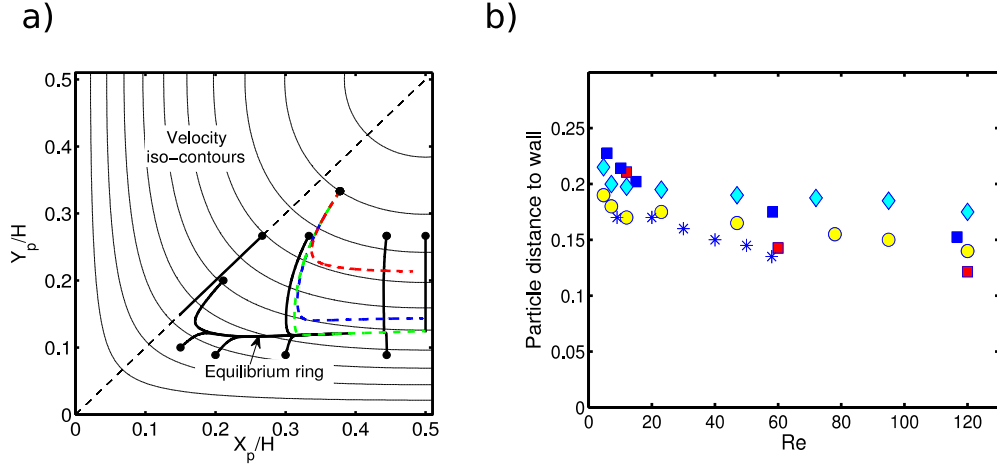


FIG. 8. (a) The trajectories of individual particles projected onto the velocity gradient plane, perpendicular to the direction of flow (in one quarter of the total cross-section). The solid circles are the initial positions of each trajectory. The thick black lines are the projection of particle trajectories for  $Re = 120$ . The dark, mid, and light gray dashed lines (red, blue, and green online) are the respective trajectories for  $Re = 12, 60,$  and  $120$  launched from the same initial position. (b) Evolution of the distance to the closest wall of the equilibrium position (scaled by  $H$ ) versus  $Re > 5$  at  $d_p/H = 0.11$ . Darker gray and lighter gray (blue and red online) squares are experimental and numerical results from the present work. Circles and diamonds are from Choi *et al.*<sup>4</sup> for  $d_p/H = 0.075$  and  $0.16$ . Stars are from Kim and Yoo<sup>22</sup> for  $d_p/H = 0.071$ .

the diagonal and midline planes do not exhibit cross-lateral migration because these are symmetry planes. Additionally, Figure 8(a) reveals that if the motion of a particle located in the diagonal plane undergoes a slight perturbation (for instance, an external force was applied on the particle during a short time), the particle moves out of the diagonal plane and follows a path (projected onto the cross-section) similar to that of a randomly seeded particle. This finding does not match the numerical results of Chun and Ladd<sup>10</sup> despite the close Reynolds numbers considered ( $Re = 100$  in their work). The origin of the discrepancy is explained later in Figure 9.

Figure 8(a) also shows the trajectories of a particle seeded at the same initial position but at different flow Reynolds numbers ( $Re = 12, 60,$  and  $120$ ). This figure reveals an auto-similarity, at different  $Re$ , of particle displacement in the cross-section. When  $Re$  decreases, the equilibrium ring shifts away from the channel wall. The particle reaches equilibrium at the midline of the channel walls. The distance between the particle equilibrium position and the channel wall (for  $Re > 5$ ) is displayed in Figure 8(b), in addition to the experimental points. The steepest evolution of this equilibrium distance happens at moderate inertia ( $Re < 20$ ). In general, a good agreement is observed with other experimental and numerical results obtained at close operating conditions. The capture of this equilibrium distance seems to be robust and depends relatively little on the technique implemented.

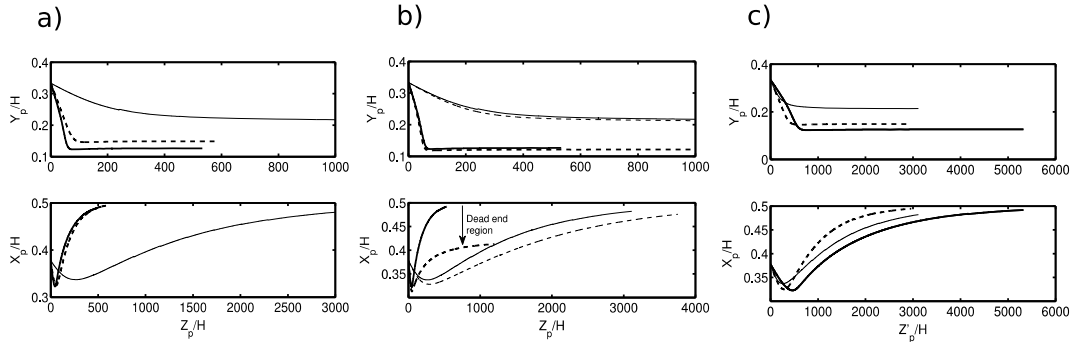


FIG. 9. Particle trajectories in the two streamwise planes, at different Reynolds numbers. (a) The length of the computational domain is  $L = 14.4d_p$ . Thin solid, dashed, and thick solid lines are for  $Re = 12, 60,$  and  $120$ . (b) The trajectories correspond to  $L = 14.4d_p$  (solid) and  $L = 7.2d_p$  (dashed). Thin and thick lines are for  $Re = 12$  and  $120$ , respectively. (c) The same trajectories as in (a) are presented in function of the stretched streamwise position  $Z'_p = Z_p Re / 12$ .

The projections of the trajectories onto the flow-velocity gradient planes ( $z,x$ ) and ( $z,y$ ) are plotted in Figure 9(a). Lateral migration takes place as long as the coordinate  $Y_p$  of the particle decreases. Cross-lateral migration occurs as long as  $X_p$  increases from a minimum value asymptotically up to  $x/H = 0.5$  (the center of the channel face).

### A. Influence of the domain length

The impact of the channel length on the particle trajectories was tested using shorter and longer channels ( $9 \times 9 \times 7.2$ )  $d_p^3$  and ( $9 \times 9 \times 20$ )  $d_p^3$ , respectively. The error committed on the particle trajectories when the domain length is increased from 14.4 to 20  $d_p$  was less than 0.4%. However, the shorter domain size has a significant influence on the particle trajectories especially at stronger flow inertia. Figure 9(b) suggests that lateral and cross-lateral migration stages are only slightly influenced by the channel length at  $Re = 12$  whereas, at  $Re = 120$ , the particle cross-lateral migration is slower in the short domain. The particle motion in the  $x$  direction is restrained when the particle approaches a zone close to the midline of the channel face, named here the “dead-end region” because the cross-lateral velocity drops to zero in this region, regardless of the particle path history.

The constraint applied to the cross-lateral motion increases with the flow inertia, because the viscous dissipation of the downstream perturbation generated by the particle becomes weaker, leading the particle to interact regularly with the “wake” of its periodic image. Also Shao *et al.*<sup>20</sup> observed that the box length had an impact on the particle equilibrium position in a tube flow, especially at high Reynolds numbers. We performed other tests with very short simulation domain length at  $Re = 120$ , and the results revealed that the particle can be pushed towards the channel corner instead of the midline of the channel face if the domain is very short. This explains the results reported in the work of Chun and Ladd<sup>10</sup> who employed a periodic channel length of  $5d_p$  for their simulations at  $Re = [100-1000]$ . If the interaction of a particle with its image can be likened, to a certain extent, to the interaction in a dilute suspension flow between two particles, one behind another in the streamwise direction (chain-like structures as those observed in tube flows), in this case, the cross-lateral migration of the downstream particle can be influenced by the wake of the upstream one. The hydrodynamic interactions could then be the possible reason for which some particles are spread along the equilibrium ring (in the experiments at  $Re = 120$  and  $z/H = 1000$ ), although theoretically, they should be all present at the midline attractor point at such a far distance from the channel inlet. Similarly, Choi *et al.*<sup>9</sup> found a probability of particle presence near the midline plane closer to 0.6 instead of 1 at  $Re = 120$  and  $z/H = 640$ .

### B. Migration streamwise length scaling

From Figure 9(a), one can estimate that the end of the first migration stage takes place at  $L_1/H \approx 50, 100, \text{ and } 500$ , respectively, for  $Re = 120, 60, \text{ and } 12$ . Then, the end of the second migration stage is achieved after a streamwise length (from the channel inlet)  $L_2/H \approx 1000$  at both  $Re = 60$  and  $120$  (which is in agreement with the experimental observation of the peak at  $Re = 120, y/H = 0.25, \text{ and } z/H = 1000$ ), and  $L_2/H \approx 3000$  at  $Re = 12$ . The prediction of the length required to reach equilibrium ( $L_1$  and  $L_2$ ) is especially important for microfluidic applications related to liquid-solid separation. To predict  $L_1$ , the usual approach assumes that particles travel towards the equilibrium positions a lateral distance that is proportional to the streamwise position and to the fractional lateral migration velocity (ratio between lateral and streamwise velocity). The cross-streamline migration velocity is classically written as  $\left[ \frac{U_m}{\langle U \rangle} = \frac{4}{3\pi} Re \frac{d_p^3}{H^3} f_c \right]$ , where  $f_c(X_p, Y_p, Re)$  is a lift coefficient that depends on  $Re$  and on the position of the particle in the cross-section (calculated by Asmolov<sup>5</sup> in plane Poiseuille flow for the case  $Re_p \ll 1$ ). For a finite particle size, the lift coefficient depends on the particle position in the cross-section and on the Reynolds number. However, researchers working on microfluidic design rules assume a constant lift coefficient.<sup>6</sup> With a constant lift coefficient, the channel length required to achieve lateral migration scales as  $\left[ \frac{H}{Re} \left( \frac{d_p}{H} \right)^2 \right]$ . At a fixed

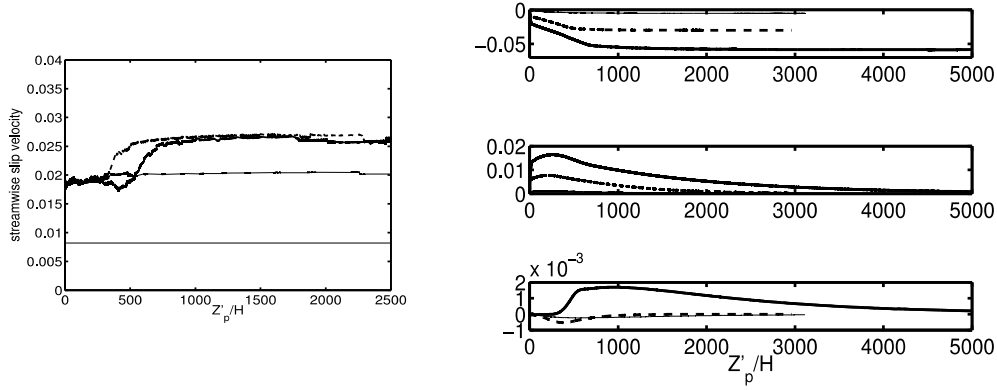


FIG. 10. (a) Magnitude of the particle slip velocity with respect to the unperturbed local flow scaled by the average flow velocity. The horizontal line is from the Faxen law  $[U_m/3(d_p/H)^2]$ , where  $U_m$  is the maximum velocity. (b) Particle rotational slip velocity scaled with  $\langle \gamma \rangle$  the average flow shear rate. From the top to the bottom:  $(\Omega_x - \omega_x)/\langle \gamma \rangle$ ,  $(\Omega_y - \omega_y)/\langle \gamma \rangle$ , and  $\Omega_z/\langle \gamma \rangle$ . In these expressions,  $\Omega$  and  $\omega$  indicate the particle and unperturbed fluid rotational velocity, respectively. In (a) and (b), thin, dashed, and thick lines are for  $Re = 12, 60,$  and  $120$ .

particle-to-channel size ratio ( $d_p/H$ ), the particle trajectories obtained in this work can inform on whether the scaling with  $Re^{-1}$  holds true in the case of finite  $Re_p$  and square channel flow instead of Poiseuille flow. Therefore, in Figure 9(c), the particle trajectories are displayed with respect to a stretched streamwise position  $Z'_p = Z_p Re/12$ , where the 12 corresponds to the minimal  $Re$  considered in the numerical simulations. The stretched plots of the trajectories match each other only during the first migration stage. This points out that the  $Re^{-1}$  scaling of the focusing length, which was originally written in the limit of low  $Re_p$ , is acceptable for the case of a finite particle size (and hence finite  $Re_p$ ) during the cross-streamline migration stage. Recall that this scaling is only valid in situations where particle interactions are suppressed. In the second migration stage, not only the  $Re^{-1}$  scaling of the streamwise migration length is not valid but also the dependence seems not to be monotonous.

### C. Particle slip

In parabolic Stokes flow, a finite sized particle exhibits only streamwise translational slip velocity with respect to the local unperturbed flow that scales as  $(d_p/H)^2$  (Faxen correction law). Finite flow inertia promotes translational and rotational particle slip, and therefore it is interesting to understand how the slip velocity is correlated with the different migration stages in the square channel. The streamwise slip velocity between the particle and the unperturbed local flow is shown in Figure 10(a). The translational particle slip seems to be independent of  $Re$  during the cross-streamline migration. At the end of the first migration stage, the slip velocity increases suddenly only at high  $Re$  and remains constant in the second migration stage.

Figure 10(b) shows that the particle rotates, and the slip in all directions is finite during the migration process. The particle rotation is slower (respectively, faster) than the flow rotational velocity in the x (respectively, y) wall direction. In addition, the particle rotation in the streamwise direction does not vanish like in the case of Stokes flow. In both x and y directions, the slip during the cross-streamline migration is non-linearly enhanced when the Reynolds number increases. During the cross-lateral migration, the particle moves keeping constant rotational slip in the direction of the nearest wall, while minimizing the slip in the other directions. A last interesting point to note is the sign change of the streamwise rotation when the Reynolds number is increased from 60 to 120.

### D. Particle-induced velocity perturbation

Figure 11 displays the particle-induced velocity perturbation in the particle median plane during the cross-streamwise migration (in (a)) and when the particle is at equilibrium (in (b)). The

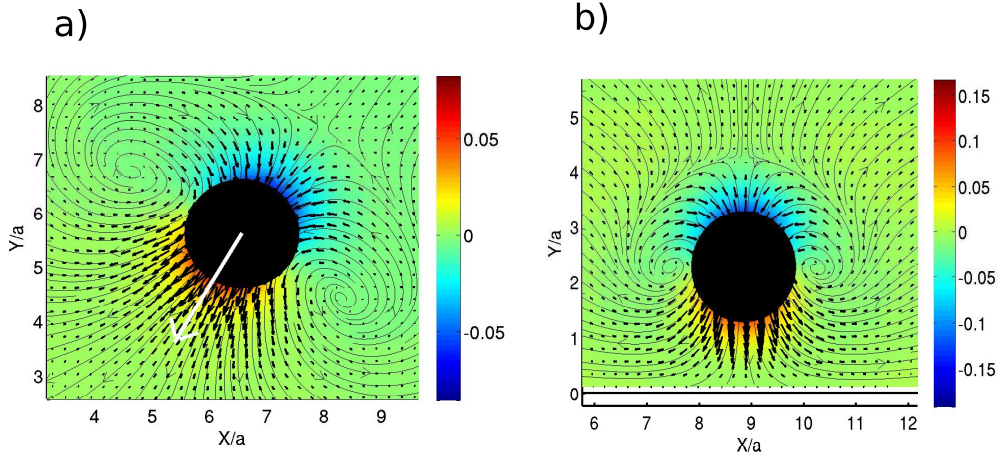


FIG. 11. Velocity perturbation (in the cross-section particle median plane) induced by the particle at  $Re = 120$ , (a) during the cross-streamwise migration stage and (b) when the particle reaches the equilibrium position. The field is color-coded by the streamwise velocity fluctuation with respect to the unperturbed field.  $a$  is the particle radius. The white arrow indicates the direction of the particle velocity in the cross-section plane.

velocity perturbation is calculated by subtracting the unperturbed component from the local velocity field. It is not symmetric with respect to the particle motion in the cross-section. Secondary flows are generated around the particle. These secondary flows are directly related to gradients in normal stress differences induced by the particle Stresslet components. Unlike the Stokes flow case, the normal stresses generated by a single particle are finite at finite flow inertia and their magnitude increases with  $Re$ .<sup>13,14</sup> The secondary flows may play an important role on the interaction between particle trajectories in the frame of multi-body hydrodynamics at finite solid volumetric concentration.

## V. CONCLUSION

The migration of finite sized neutrally buoyant particles in square channel flow was investigated in this paper. When the Reynolds number was increased from 0.07 to 120, experimental measurements of particle distributions in the channel cross-section revealed that the particle cross-streamline motion exhibits two distinct regimes. At relatively high Reynolds numbers ( $Re \geq 10$ ), the particle migration induced by inertial lift forces is oriented towards the channel walls. At low Reynolds numbers, the inertial forces being weak, the particles move towards the channel center, even at low concentration, seemingly due to shear-induced multi-body interactions. The process is slow, and consequently a length of several thousand channel heights is required to observe the establishment of the particle distribution. That is probably why such observation was never reported (to the author's knowledge) in previous experiments. With the concentration and particle-to-channel size ratio considered for this work, the transition between both regimes takes place in the range  $Re = [1-10]$ . The transition range shifts towards higher Reynolds numbers when the concentration or particle size is increased.

Full trajectories of freely moving particles in the square channel flow were described in the inertial regime ( $Re = [10-120]$ ), thanks to numerical simulations. The particle trajectories revealed, in agreement with previous studies, that the migration occurs in two stages and that the first (cross-streamline) stage is much faster than the second (cross-lateral) one. We showed that the equilibrium positions in a diagonal plane are unstable to perturbations perpendicular to that plane, and that only the midline of the channel walls are stable point attractors. The particle-induced normal stresses trigger secondary flows around the particle during the migration stages and at equilibrium. The rotational perturbation of the flow, taking longer time to be dissipated at higher Reynolds numbers, might play a crucial role in the (hydrodynamic) interaction between particles and control the relative particle positions in the train-like structures observed in inertial tube flows<sup>20,21</sup> (at low but finite solid volumetric concentration).

Finally, it would be interesting to carry further investigation on the effect of the particle-to-channel size ratio on the particle trajectory (varying the particle Reynolds number for a fixed channel Reynolds number). The numerical method used here is valid for finite but not very large particles in a channel, owing to the truncation of the multipole expansion after the second order term (i.e., the quadrupole term becomes important when the flow strain rate variation within the particle volume is significant). Rigorous information might be obtained in the future thanks to the development of 3D real time particle tracking techniques, as well as the increasing computational performance of the direct numerical simulation methods for finite sized particles in confined flows.

## ACKNOWLEDGMENTS

This work was granted access to the HPC resources of CALMIP and GENCI (TGCC/CINES/IDRIS) under the allocations 2014-P1002 and i20142b694, respectively. The authors would like to thank P. Duru for his help to adjust the experimental technique and E. Climent for his comments on the first draft of the manuscript.

- <sup>1</sup> G. Segré and A. Silberberg, “Behaviour of macroscopic rigid spheres in Poiseuille flow: Part 1, Part 2. Experimental results and interpretation,” *J. Fluid Mech.* **14**, 136–157 (1962).
- <sup>2</sup> B. P. Ho. and L. G. Leal, “Inertial migration of rigid spheres in two-dimensional unidirectional flows,” *J. Fluid Mech.* **65**, 365–400 (1974).
- <sup>3</sup> P. Vasseur and R. G. Cox, “The lateral migration of a spherical particle in two-dimensional shear flows,” *J. Fluid Mech.* **78**, 385–413 (1976).
- <sup>4</sup> J. A. Schonberg and E. J. Hinch, “Inertial migration of a sphere in Poiseuille flow,” *J. Fluid Mech.* **203**, 517–524 (1989).
- <sup>5</sup> E. S. Asmolov, “The inertial lift on a spherical particle in a plane Poiseuille flow at large channel Reynolds number,” *J. Fluid Mech.* **381**, 63–87 (1999).
- <sup>6</sup> J. P. Matas, J. F. Morris, and E. Guazzelli, “Lateral force on a rigid sphere in large-inertia laminar pipe flow,” *J. Fluid Mech.* **621**, 59–67 (2009).
- <sup>7</sup> D. Di Carlo, “Inertial microfluidics,” *Lab Chip* **9**, 3038–3046 (2009).
- <sup>8</sup> A. A. S. Bhagat, S. S. Kuntaegowdanahalli, and I. Papautsky, “Enhanced particle filtration in straight microchannels using shear-modulated inertial migration,” *Phys. Fluids* **20**, 101702 (2008).
- <sup>9</sup> Y.-S. Choi, K.-W. Seo, and S.-J. Lee, “Lateral and cross-lateral focusing of spherical particles in a square microchannel,” *Lab Chip* **11**, 460–465 (2011).
- <sup>10</sup> B. Chun and A. J. C. Ladd, “Inertial migration of neutrally buoyant particles in a square duct: An investigation of multiple equilibrium positions,” *Phys. Fluids* **18**, 031704 (2006).
- <sup>11</sup> D. Di Carlo, J. F. Edd, K. J. Humphry, H. A. Stone, and M. Toner, “Particle segregation and dynamics in confined flows,” *Phys. Rev. Lett.* **102**, 094503 (2009).
- <sup>12</sup> S. Lomholt and M. R. Maxey, “Force-coupling method for particulate two-phase flow: Stokes flow,” *J. Comput. Phys.* **184**, 381–405 (2003).
- <sup>13</sup> V. Loisel, M. Abbas, O. Masbernat, and E. Climent, “The effect of neutrally-buoyant finite-size particles on channel flows in the laminar-turbulent transition regime,” *Phys. Fluids* **25**, 123304-1–123304-18 (2013).
- <sup>14</sup> D. Mikulencak and J. Morris, “Stationary shear flow around fixed and free bodies at finite Reynolds number,” *J. Fluid Mech.* **520**, 215–242 (2004).
- <sup>15</sup> F. P. Bretherton, “The motion of rigid particles in a shear flow at low Reynolds number,” *J. Fluid Mech.* **14**, 284–304 (1962).
- <sup>16</sup> R. Phillips, R. Armstrong, R. Brown, A. Graham, and J. Abbott, “A constitutive equation for concentrated suspensions that accounts for shear induced particle migration,” *Phys. Fluids* **4**, 30–40 (1992).
- <sup>17</sup> M. Han, C. Kim, M. Kim, and S. Lee, “Particle migration in tube flow of suspensions,” *J. Rheol.* **43**(5), 1157–1174 (1999).
- <sup>18</sup> D. Semwogerere, J. F. Morris, and E. Weeks, “Development of particle migration in pressure-driven flow of a Brownian suspension,” *J. Fluid Mech.* **581**, 437–451 (2007).
- <sup>19</sup> Note that in the concentrated case, the particle distribution in the channel center is thicker than a Dirac delta function. Some particle aggregation was observed (doublets or triplets formation) after the particles traveled towards the center, knowing that we checked the absence of aggregation in the region at the vicinity of the channel inlet for all run cases.
- <sup>20</sup> X. Shao, Z. Yu, and B. Sun, “Inertial migration of spherical particles in circular Poiseuille flow at moderately high Reynolds numbers,” *Phys. Fluids* **20**, 103307-1–103307-11 (2008).
- <sup>21</sup> J. P. Matas, V. Glezer, E. Guazzelli, and J. F. Morris, “Trains of particles in finite-Reynolds-number pipe flow,” *Phys. Fluids* **16**(11), 4192–4195 (1994).
- <sup>22</sup> Y. W. Kim and J. Y. Yoo, “The lateral migration of neutrally buoyant spheres transported through square microchannels,” *J. Micromech. Microeng.* **18**, 065015 (2008).